Proceedings of ASME Turbo Expo 2007
Power for Land, Sea, and Air
May 14–17, 2007, Montreal, Canada

GT2007-28158

DYNAMICS, NOX AND FLASHBACK CHARACTERITICS OF CONFINED PRE-MIXED HYDROGEN ENRICHED METHANE FLAMES

Onur Tuncer
Turbine Innovation & Energy Research Center
Department of Mechanical Engineering
Louisiana State University
Baton Rouge, LA, 70803

Sumanta Acharya*
Turbine Innovation & Energy Research Center
Department of Mechanical Engineering
Louisiana State University
Baton Rouge, LA, 70803

Jong Ho Uhm
Turbine Innovation & Energy Research Center
Department of Mechanical Engineering
Louisiana State University
Baton Rouge, LA, 70803

ABSTRACT

The operating regime of a gas turbine combustor is highly sensitive to fuel composition changes. In particular, the addition of hydrogen, a major constituent of syngas, has a major effect on flame behavior due to the higher burning rates associated with hydrogen. A laboratory scale pre-mixed test rig is constructed in order to study such effects. The fuel composition is incremented with increasing hydrogen starting from 100% methane. It is observed that increased RMS pressure levels and higher susceptibility to flashback occurs with increasing hydrogen volume fraction. Furthermore, hydrogen enrichment can cause an abrupt change in the dominant acoustic mode. Phase locked hydroxyl PLIF measurements have been performed with respect to the dominant acoustic instability limit cycle. These measurements are complemented with real time heat release, emissions and flashback measurements. Particular emphasis is put on time resolving the thermo-acoustic instability induced flashback cycle of the wedge-shaped flame front and the temporal events associated with flashback.

INTRODUCTION

Modern premixed gas turbine combustors are usually operated near the lean blowout limit due to emission requirements [1]. Lean premixed combustion decreases the adiabatic flame temperature thus reducing the production rate of nitric oxides which is highly temperature dependent [2]. In this operating range flame holding and thermo-acoustic instability become the two most important considerations. Thermo-acoustic instability not only deteriorates the material structure of the combustor subjecting it to fatigue loading [4], but also can induce flashback into the pre-mixing section [3]. Lean premixed natural gas combustion has been extensively studied; however, as the transition is made from natural gas to hydrogen-enriched fuels (e.g., syngas), the impact of hydrogen addition on the key performance metrics is not well understood. Therefore, near lean blowout behavior of syngas needs to be explored in a detailed manner.

Thermo-acoustic oscillations occur because unsteady heat release couples positively with sound waves producing large velocity and pressure perturbations [4]. If the unsteady heat input is in phase with pressure perturbations acoustic waves gain energy and instability takes place. Strength of these oscillations are limited by non-linear effects such as fuel consumption rates, and limit cycle oscillations occur. However, these oscillations can be sufficiently strong that they can cause gas turbines to shut down or cause hardware damage. If the pressure oscillations are strong enough they can cause the flame to enter into the premixing section triggering flashback. This phenomenon is called as thermo-acoustic instability induced flame flashback.

Synthesis gas is a variable mixture of primarily hydrogen (H_2) and carbon monoxide (CO). Depending on the gasification process variables, and which solid is gasified, substantial changes in the resulting syngas composition occurs [5]. These changes in the syngas composition can significantly alter the flame behavior [6]. Therefore, the composition of the fuel impacts the turbine life and emissions [7], and characterization of the flame behavior at different fuel compositions is an

*Corresponding author, acharya@me.lsu.edu

important task. Furthermore, syngas combustion is prone to flashback due to high flame speeds associated with its hydrogen content. Under atmospheric conditions the flame speed of a stoichiometric methane air mixture is about 40 cm/s whereas that of a hydrogen air flame is about 200 cm/s. Therefore, hydrogen flame propagates five times faster than a methane flame under atmospheric pressure. This mismatch between flame speeds leads to flame holding problems in a gas turbine engine environment.

To achieve a desired power output from syngas, high volumetric flow rates are needed due to the lower heating value of the fuel per unit volume. High volumetric flow rates translate into higher axial speeds inside the pre-mixer. This axial velocity tries to push the flame away from its anchoring point (i.e. the center-body in this particular case) at the dump plane which poses significant problems with respect to flame holding and can yield to a complete blow-off [8,9,10]. In this paper, we present measurements with hydrogen enriched natural gas, and examine the role of hydrogen addition on the performance of the gas turbine combustor. By taking advantage of the single mode limit cycle oscillations, the phase resolved behavior of the unsteady processes (thermo-acoustics and flashback) can be examined.

EXPERIMENTAL SETUP

Figure 1 shows a schematic of the experimental setup that includes the combustor, gas bottles, metering systems, and the instrumentation. The combustor system consists of the combustor shell, the inlet fuel and air-delivery system, and the premixing section. The combustor shell is comprised of two pieces (see Figure 2 and Figure 3). A 2.75" inner diameter quartz tube sits on a stainless steel flange that defines the dump plane. Quartz tube enables optical access into the main re-circulation zone. The basic design of the fuel-air premixing section represents a generic configuration with characteristic features similar to industrial gas turbine systems. More detailed discussion about the design of this specific combustor can be found in [11, 12]. Combustor exit is only restricted not fully choked. Combustor is operated up to a power rating of 20 kW. Quartz tube and the stainless steel shell are cooled on the outer wall by means of forced convection air-jets during combustion.

Combustion air is fed through an eight-blade 45°-swirl vane (see Figure 3). A correlation [13] gives the corresponding swirl number as Sw=0.98. Swirl provides stabilization at the dump plane and facilitates the entrainment of fuel jets within the cross flow at the pre-mixer. Fuel jets are injected radially outwards. Centrbody (which is also the fuel injector) is inline with the dump plane to provide aerodynamic flame stabilization.

Hydrogen H_2 and methane CH_4 gases are individually supplied from compressed tanks and mixed within a manifold prior to combustor inlet (see Figure 1). Their flow rates are controlled by separate mass flow meters. Mass flow rates are adjusted separately in order to achieve the desired fuel composition. Air necessary for combustion is supplied from a 19.7atm, 0.2 Nm^3/s air compressor. Volumetric airflow rate is measured by a rotameter, and a pressure gage at the rotameter exit is used to correct the readings.

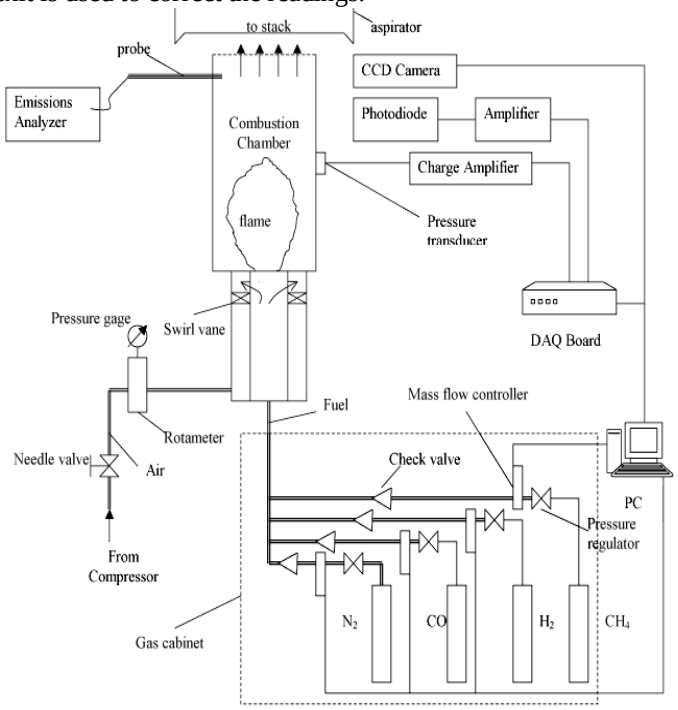

Figure 1 Schematic of Experimental Setup

RESULTS AND DISCUSSION

Unlike natural gas, synthesis gas flame has a much different behavior due to different laminar flame speed and adiabatic flame temperature. Both the laminar flame speed and adiabatic flame temperature heavily depend on mixture composition. Since there are multiple fuels in a methane and hydrogen mixture a suitable definition of the equivalence ratio, which takes the overall stoichiometry into account, is needed. Following the assumptions made by Yu et. al. [14] an equivalence ratio is defined as follows (see Eq. 1). This equation assumes that the hydrogen in the blend is completely oxidized and the remaining oxygen is used to burn the methane content. This is a reasonable assumption since the hydrogen oxidation proceeds much faster than methane oxidation.

$$\phi = \frac{C_F / \left[C_A - C_H / (C_H / C_A)_{st} \right]}{(C_F / C_A)_{st}} \qquad (1)$$

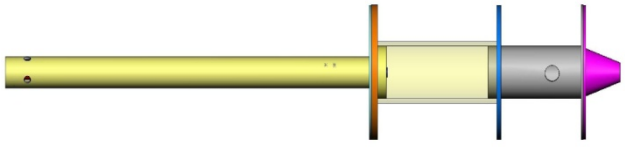

Figure 2 Overall View of the Combustor

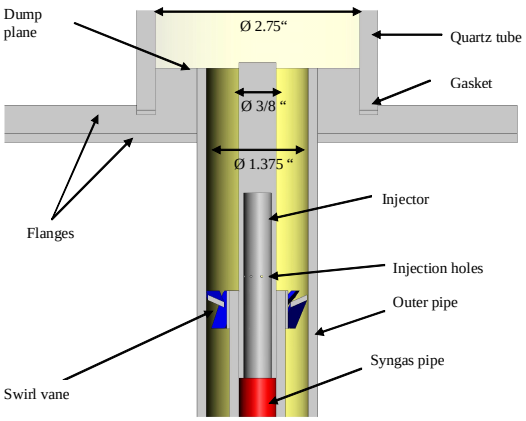

Figure 3 Close-Up View of the Fuel Delivery Section

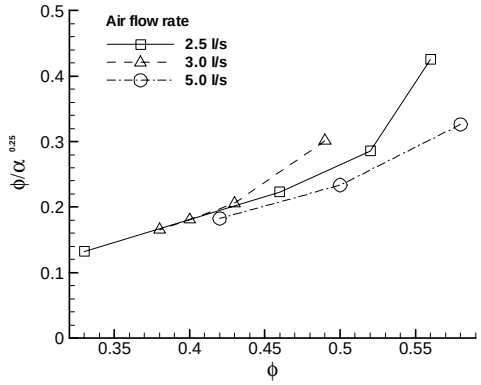

a. Parametric Relations at Blowout

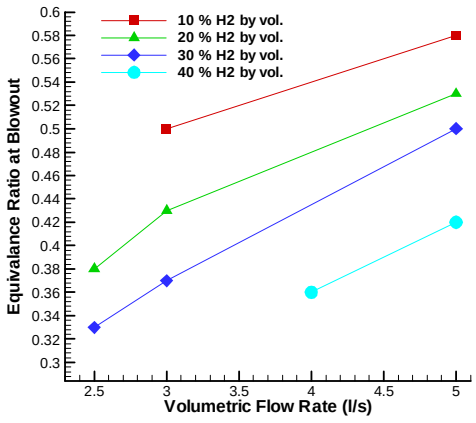

b. Effect of Hydrogen Enrichment on Blowout

Figure 4 Lean Blowout Limits as a Function of Percent Hydrogen Volume Fraction (α)

Lean Blowout (LBO) Measurements

Gas turbine engines are operated near their lean blow-off limits due to emissions considerations. Hydrogen enrichment considerably extends the lean blowout limits of the methane fuel, and evidence of this is shown in Figure 4. These effects regarding the extension of lean blowout limits through hydrogen addition are consistent with the recent observations reported by [15, 16, 17]. In Figure 4a, a scaled LBO parameter $\phi/\alpha^{0.25}$, which is obtained empirically, is shown. By using this parameter data recorded at different air flow rates reasonable scaling is observed especially for low equivalence ratios $\phi \le 0.5$. Beyond this point some scatter in the data is observed. As seen in Fig. 4, hydrogen enrichment extends the LBO limit quite extensively. It is also observed that for hydrogen enriched methane LBO equivalence ratio is not fixed, it both depends on the extent of enrichment and on the flow rate as shown in Figure 4b. At higher flow rates higher hydrogen content was necessary to sustain the flame. Equivalence ratio at lean blowout increases as the volumetric flow rate (hence fluid velocity) increases for all fuel compositions.

In flamelet combustion regime blowout occurs when the local flame speed is less than the oncoming fluid velocity everywhere in the flame. Thus the stabilization mechanism for flamelet-like combustion is based on the flame front propagation [17]. Turbulent flame speed is often expressed in terms of laminar flame speed multiplied by a function which depends both on turbulence intensity and geometry. For all conditions tested in the laboratory combustor, the geometry is fixed, so those can be factored out when correlating the blow out behavior. Assuming turbulence intensities are similar as a first order approximation the loading parameter can be expressed in terms of the laminar flame speed of the fuel mixture. For a two-fuel blend one can express flame speed as a sum of individual species' flame speed weighted by their mole fractions inside the fuel blend (Eq. 2) as a first order approximation.

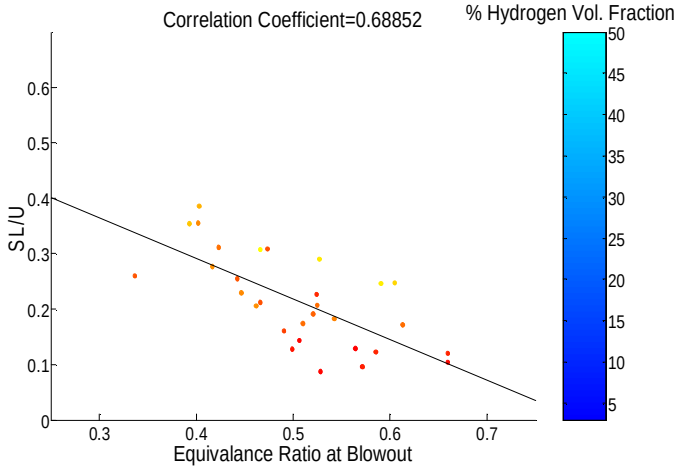

Figure 5 Relationship Between Blowout Equivalence Ratio and Flamelet Based Loading Parameter

$$S_L = \frac{C_F}{C_F + C_H} S_{L,CH_4,\phi} + \frac{C_H}{C_F + C_H} S_{L,H_2,s} \qquad (2)$$

Note that the flame speed of hydrogen is considered at stoichiometric conditions due to the same assumptions made for the definition of the equivalence ratio. Flame speed of methane on the other hand depends on the equivalence ratio calculated from Eq. 1. Consequently, the flame speed of the mixture is calculated using the above equation. Hydrogen/methane flame chemistry is simply too complex to be mapped out by simple curve fits such as this one used here article. This is nevertheless an over simplified first order approximation to the flame speed. Results are demonstrated in Figure 5. This figure shows the relationship between lean blowout equivalence ratio and flamelet based loading parameter. Data for blowout is recorded in a wide range of operating conditions $2.5 \le \dot{Q}_{air} \le 7.1 l/s$, $0.4 \le \phi \le 1.3$ as well as a wide range of fuel compositions (from pure methane to 50% methane/50 % hydrogen with the hydrogen concentrations indicated by the color map). As it can be seen from this figure data points are roughly correlated by a single line with a correlation coefficient of 0.69.

Chemical time scales for hydrogen and methane oxidation are quite different. Therefore considering the turbulence in practical combustors, combustion process can indeed cover a wide spectrum of Damköhler numbers. Another reactor loading parameter L_2 based on a well stirred reactor approach can be defined as well (Eq. 3). Following the work of Hoffman et. al. [18], azimuthal velocity component U_θ and combustor diameter D are used as the appropriate scaling parameters. Here α denotes the thermal diffusivity of the reactant mixture. The thermal diffusion coefficient of the mixture is calculated using the thermal diffusion coefficients of individual species (air is treated as a single species within the calculation).

$$L_2 = \frac{\alpha U}{S_L{}^2 D} \tag{3}$$

Results for reactor based correlation are shown in Figure 6. For this parameter L_2 however, correlation is weaker compared to the flame speed correlation. The correlation coefficient is only 0.41. Especially for low hydrogen content mixtures (shown with darker spots on the plot) one observes that there is a very large scatter in the data. This in turn points out that well-stirred reactor based loading does not offer a good explanation

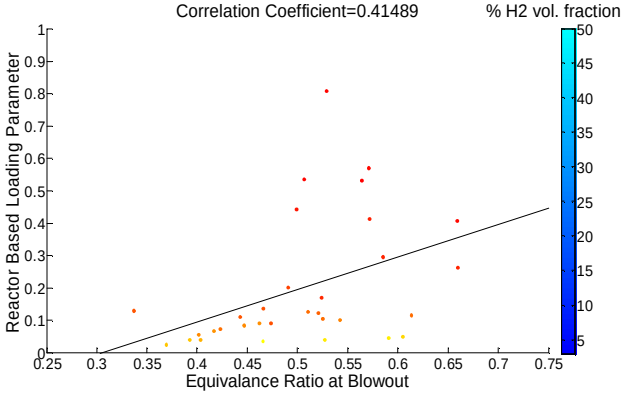

Figure 6 Relationship Between Blowout Equivalence Ratio and Reactor Based Loading Parameter

for methane rich mixtures. On the other hand, one can see that for hydrogen rich mixtures (indicated with lighter shades) data seems to correlate better with this loading parameter. More discussion on this issue will be provided at a later section while discussing PLIF measurement results. A "perfectly stirred reactor" is an idealized scenario and does not necessarily apply laboratory or industrial scale gas turbine burners even in the presence of a strong re-circulation vortex in the primary reaction zone. Had it been possible to characterize swirl stabilized gas turbine burners as "well stirred reactors" much of the problems that are being researched today would have been simply trivial in nature and no research would have been necessary. Well stirred reactor approach on the other hand provides the researchers with an idealized scenario to use as a benchmark for their results.

Pressure, Heat Release and Flashback Measurements

Six Kistler 7061 water-cooled piezo-electric pressure transducers are mounted along the combustor wall, and measure dynamic pressure variations in the combustor. In order to examine the waveform of the combustion instability pressure inside the reactor is measured at several stations along the entire length of the combustor.

Figure 7 shows the scaling of RMS pressure levels which is linked to the amplitude of the combustion generated noise. Data points shown in the scatter plot covers a wide parameter space (i.e. equivalence ratio, flow rate and mixture composition). Data points showing extinction re-ignition behavior near the lean blowout limit are typically characterized by high amplitude pressure fluctuations. These points are not shown in this plot as these belong to an entirely different regime. Combustion generated noise typically depends on Mach number and flame dilatation ratio. Flame dilatation ratio is defined as the temperature ratio of burned gases to the unburned reactants. Combustion noise has a quadratic dependence on the flame dilatation ratio. For the Mach number, combustion generated noise has a fourth power dependence. Correlation coefficient of the linear trendline fitted to the scatter points is 0.76.

The CH/OH radical light intensity is recorded using a silicon PIN photodiode (Melles-Griot) looking at the flame equipped with an appropriate band-pass optical filter. Collected light is focused onto the sensor area by a convex lens. Flashback signal is collected through a fiber optic cable which is mounted at the premixing section. There is no optical filter mounted with this photodiode radical a filter centered at 430 nm with a 10 nm FWHM transmission width is used. Photodiode reading is taken as a measure of integral heat release fluctuations in the main reaction zone of the reactor. In order to detect flame flashback a separate photodiode is used. This photodiode sees flashback and the fiber optic cable transmits light at the visible spectrum. Fiber optic cable is mounted 15 mm upstream of the combustor dump plane. When the flame enters inside the pre-mixer and travels this distance, it is seen by the photodiode and the light signal is converted into

voltage which is in turn recorded by the DAQ board along with the other signals.

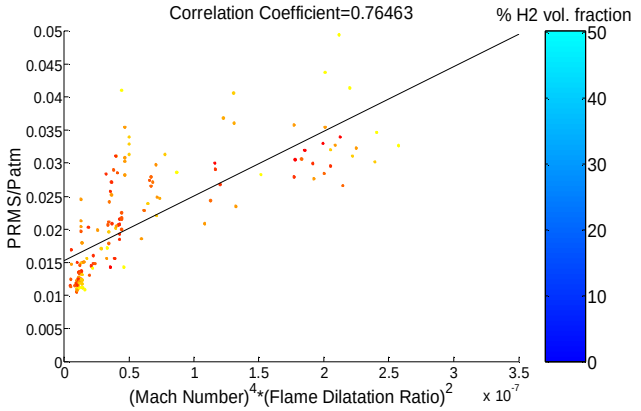

Figure 7 Scaling of RMS Pressure Level ($0.4 \le \phi \le 1.3$, $2.5 \le \dot{Q}_{air} \le 7.1\ lt/s$)

Figure 8 demonstrates the dominant frequency of combustion as a function of equivalence ratio and fuel composition. Two distinct regions of dominant mode, one with higher frequency (around 90Hz), the other one with lower frequency (around 30 Hz) can be easily identified. This transition occurs around 20-25% hydrogen content, and as will be discussed later, represents conditions where flashback is initiated. The flashback is associated with periodic low frequency fluctuations, with the flame flashing back and recovering, and these fluctuations are at the observed pressure oscillation frequency. This implies that the periodic flashback is coupling with the air-delivery-chamber/combustor acoustics with a positive feedback.

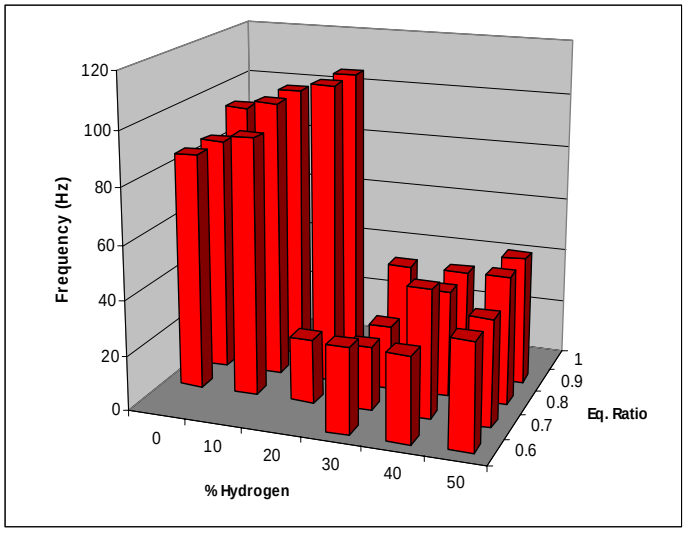

Figure 8 Dominant Frequency (Hz) with Respect to Fuel Composition and Equivalence Ratio (Q_{air}=6.2 lt/s)

Figure 9 shows the longitudinal distribution of the pressure RMS for no-hydrogen and with-hydrogen. In Figure 9, x is the distance measured from the combustor inlet, and H is the overall length of the combustor. Dump plane is located at x/H=0.6. In all cases RMS pressure decays with the stream-wise distance going from acoustically closed inlet to the acoustically open outlet. RMS pressure amplitudes increase with increasing hydrogen content. This effect is more pronounced towards the combustor exit. Although there is a sudden drop in the dominant frequency (see Figure 8) RMS pressure waveform does not experience a substantial change as seen in Figure 9.

Figure 10 shows the spectra of pressure, heat release and flashback signals on a logarithmic scale. The frequency shift associated with the hydrogen addition (Figure 8) is observed in more detail in Fig. 10. For pure methane, the flashback signal amplitude is low, and is at the noise level associated with the indirect flame radiation "(i.e. indirect optical reflections from the combustion chamber into the location where the fiber-optic cable is mounted). At 40-50% hydrogen (Fig. 10b and Fig. 10c) the flashback signal in the 40-47 Hz range is clearly evident. The flashback activity and change in the dominant frequency in the pressure oscillations accompanies one another, and are both at the same frequency. This implies that as the flame moves up and down inside the pre-mixer and generates heat release fluctuations at the flashback frequency, the resulting heat release dynamics couples with an acoustic mode of the combustor system exciting this mode. This behavior is phase resolved in a latter section of the article.

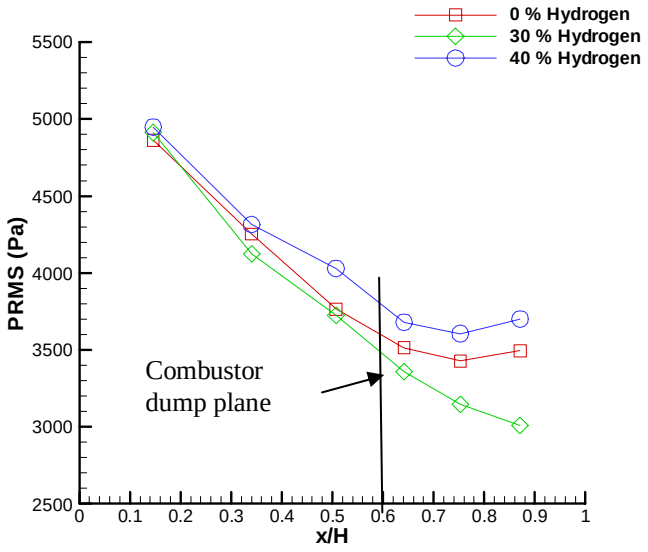

Figure 9 RMS Pressure Variation Along the Combustor Axis

Another way through which fuel composition affects the feedback route between heat release and pressure fluctuations within the thermo-acoustic loop is the change that occurs when the flame center of mass is changed due to change in flame speed. As the flame speed increases with the addition of hydrogen the flame becomes shorter and the distance to the flame center of mass (center of heat release) decreases. This yields a reduced convective time for the equivalence ratio perturbations which can cause a stable combustor to become

unstable and vice versa [22]. Figure 11 shows the change in flame center of mass with varying fuel composition while keeping the inflow velocity constant to factor out the aerodynamic effects. These are time averaged two dimensional hydroxyl chemiluminescence images captured with an intensified CCD camera equipped with an appropriate band pass filter. For each image, the CCD array is gated for 10 microseconds and a total of 400 images are recorded for averaging. One can notice the change in the location between two flow conditions tested. With 50% methane and 50% hydrogen, most of the heat release takes place in spatial locations closer to the dump plane. Inlet section, dump plane and the location fuel injector are also schematically in this figure.

Emissions Measurements

Nitric oxide emission measurements have been performed using a chemiluminescence analyzer. A water cooled probe is placed at the combustor exit. Exhaust gases are sucked at the center. Keeping the other variables constant (i.e. equivalence ratio, volumetric flow rate) and increasing the hydrogen volume fraction of the fuel results in increased nitric oxide emissions index values (see Figure 12). Note that in this figure there is only a single data point is shown for equivalence ratio for 1.0 which is depicted in blue color. Therefore blue lines do not simply disappear behind the other ones as there is only a single blue line. This is an issue which might give rise to a misunderstanding and hence is clarified here. On the other hand hydrogen enrichment enables the sustainment of combustion at much leaner equivalence ratios than those are ever possible with methane. Premixed lean combustion has long been utilized as an industry standard technique to reduce nitric oxide emissions. Even though hydrogen addition increases NO_x emissions at a fixed equivalence ratio the overall emissions still can be greatly reduced by burning leaner mixtures of methane and hydrogen blend, which were impossible for the pure methane case. This will reduce the adiabatic flame temperature further down reducing the thermal and other contribution to the total NO_x emissions index.

Figure 13 shows the correlation between adiabatic flame temperature and nitric oxide emissions index (EINO) over a wide parameter space including fuel variability effects. Points on the scatter plot are color coded according to the binary fuel mixture composition. Note that for the flow conditions tested the residence time changes by almost a factor of three. Residence time is one of the determining parameters for the equilibrium concentration of species. However, as seen in Fig. 13, the correlation of EINO with the adiabatic flame temperature is quite good, with a correlation coefficient of nearly 0.8, and one can therefore argue that the residence times are longer than the NO-formation timescales, and therefore the effects of residence time play a relatively smaller role. The increase in the nitric oxide emissions index with increasing hydrogen is potentially linked to the associated increased concentration of the hydroxyl (OH) radicals within the radical pool. Higher hydroxyl concentrations can increase the forward

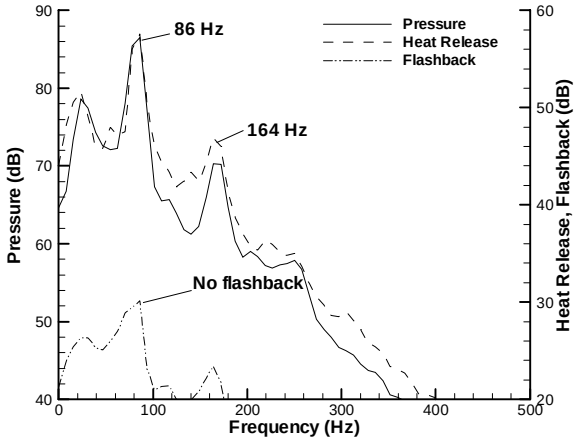

a. Pure Methane

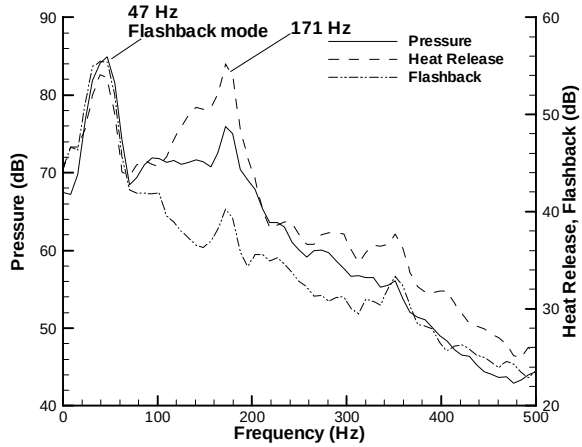

b. 40% H_2 by volume

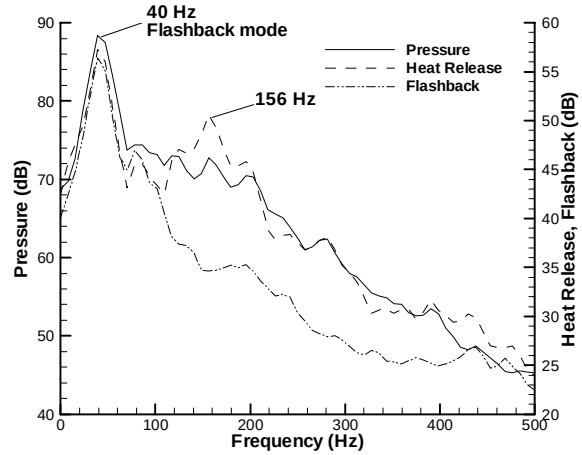

c.50% H_2 by volume

Figure 10 Pressure, Heat Release and Flashback Spectra (Q_{air}=6.2 lt/s, Φ=0.7)

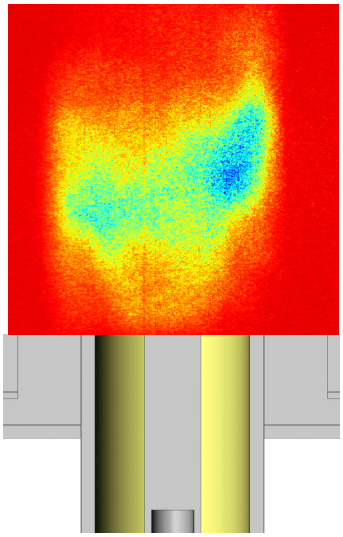

a. Pure Methane

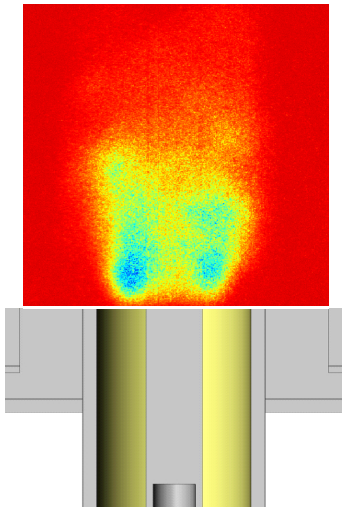

b.50 % H_2 by volume

Figure 11 OH* Chemiluminescence Images Demonstrating Effect of Fuel Composition on the Distance to the Flame Center of Mass at a Fixed Flow Rate and Equivalence Ratio (Q_{air}=6.2 l/s, Φ=0.7)

reaction rates in the nitric oxide formation mechanism involving the OH radical. However, as Figure 13 suggests the main scaling parameter is the adiabatic flame temperature. Yet, this does not mean that residence times are insignificant. In fact, most of the data scatter shown of Figure 13 is due to the effect of varying residence time. Much shorter residence times of course favor lower nitric oxide emissions due to chemical inequilibrium. If all residence times on the other hand are longer than the formation time scale of NO emissions, then emissions levels reach closer to equilibrium values. It can be therefore be concluded that the extended Zeldovich mechanism (thermal NO_x) is the dominating pathway to NO formation in this case. Residence time, albeit it has a smaller impact, should be responsible from the scatter in the data points.

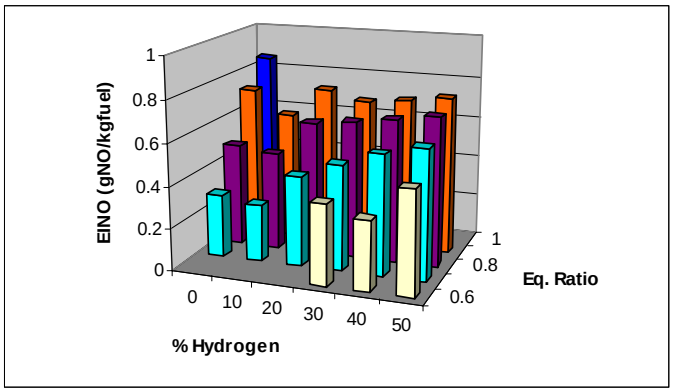

Figure 12 EINO as a Function of Equivalence Ratio and Hydrogen Volume Fraction

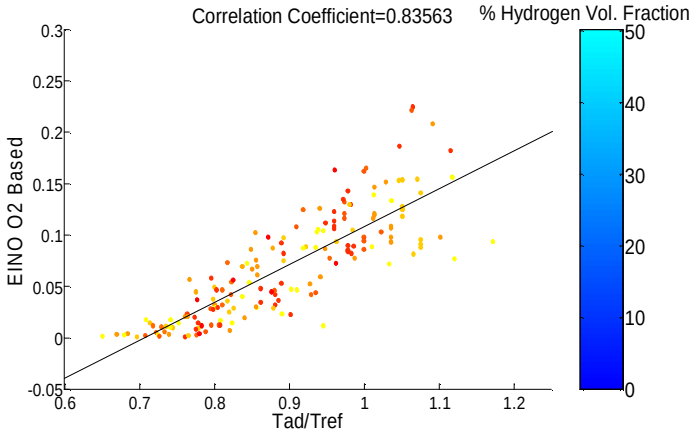

Figure 13 Relationship Between Adiabatic Flame Temperature and Emissions Index in a Wide Range of Load Conditions ($0.4 \le \phi \le 1.3$, $2.5 \le \dot{Q}_{air} \le 7.1\ lt/s$)

Figure 14 demonstrates the phase averaged behavior of pressure, heat release and flashback signals. In view of the instability, pressure and heat release signals are nearly in phase with each other resulting in a positive Rayleigh index. In Figs. 14(a) and 14(b) corresponding respectively to pure methane, and 10% hydrogen by volume, the flashback signal is flat suggesting no flashback activity at these conditions. However, in Fig. 14(c), the amplitude of the flashback signal shows a significant peak at the 90-degree phase instance with respect to the pressure instability cycle. Consequently flashback signal reaches its maximum value when the pressure is also at a maximum indicating the inter-relationship between the pressure dynamics and flashback. These observations support the earlier conclusions based on Figure 10 (i.e. no flashback with pure methane and flashback with 50% H_2/50% CH_4 mixture).

Figure 15 depicts the cycle of events leading to periodic flame flashback. As this cartoon illustrates, the attached wedge shaped flame moves upstream due to a flow reversal shortly following pressure buildup. Vertical arrows pointing upwards and downwards indicate total flow velocity (mean + acoustic)

and flame speed respectively. Whenever the flame is detached from the injector tip the flame anchoring point (tip of the wedge shaped flame) moves with a velocity which is the sum of the flame speed and fluid velocity. As it is seen from the figure at the mid-cycle flame is entirely inside the pre-mixer. As the cycle progresses and the total fluid velocity attains a positive value that exceeds the flame speed (which always points towards the reactants side flame front) recovers its shape and re-attaches to the center body tip. For a more elaborate discussion of this phenomenon (including a theoretical background) please refer to [11, 12] wherein these flame attachment and flow reversal issues are treated.

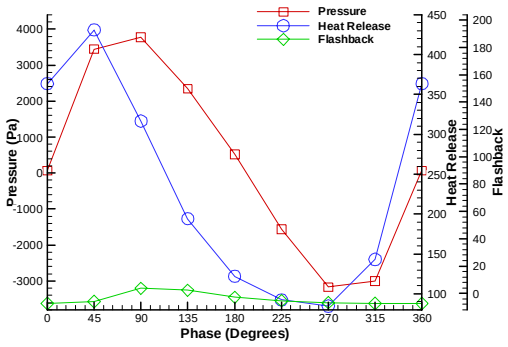

a. Pure Methane

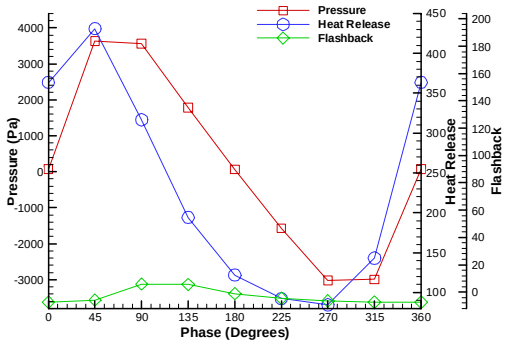

b. 10% H_2 by volume

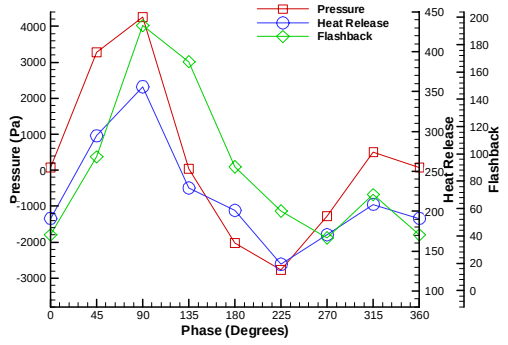

c. 50% H_2 by volume

Figure 14 Phase Averaged Pressure, Heat Release and Flashback Signals

PLIF Measurements

Planar laser induced fluorescence (PLIF) measurements for the hydroxyl radical have been conducted in order to reveal the structure of the flame front. For OH PLIF, OH radical is excited at $Q_1(7)$ transition of the $A^2\Sigma^+ \leftarrow X^2\Pi(0, 0)$ band at 281.34 nm and fluorescence is collected at the range from 306 to 320 nm. The fluorescence intensity can be qualitatively linked to OH mole fraction [21].

The experimental arrangement of the PLIF system is shown in Figure 16. Setup includes a Nd:YAG pumped dye laser, an intensified CCD camera, sheet optics and a computer controlled programmable timing unit. After passing the sheet optics, the 283.39 nm wavelength laser beam forms a sheet of approximate thickness 0.5 mm which passes through the center of the cylindrical quartz tube. The pulse energy was set to approximately 10 mJ/pulse and the pulse duration was 5 ns. An intensified ICCD camera, which has a 512 x 512 CCD array, detected the induced fluorescence images. Gate duration for the camera was set to 1000 ns during the acquisition of images. A filter ensured that only light between the wavelengths 300 – 320 nm is transmitted and all the other light rejected. Hence, OH fluorescence can be collected using UV-sensitive intensified CCD cameras. Rectangular PLIF images shown correspond to a 150 mm x 70 mm region of the flow field. Images were calibrated using a rectangular grid to correct spherical aberrations caused by the quartz cylinder that encloses the viewable portion of the flame. A peak finding scan was performed in the vicinity of 280nm - 290nm with a wavelength increment of 0.05nm. This narrow band scan is used to correct any possible detuning of the dye laser. The OH fluorescence spectra shows that the peak signal strength is observed at 283.39 nm which corresponds to a $A^2\Sigma^+ \leftarrow X^2\Pi(0, 0)$ electronic transition of the hydroxyl radical.

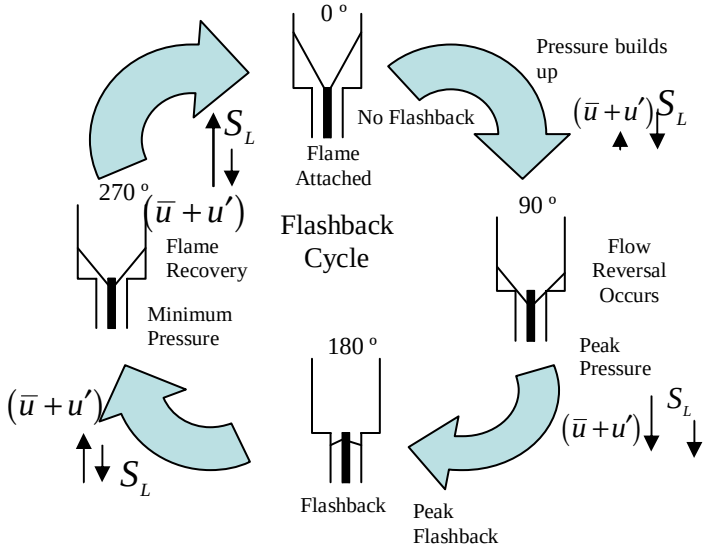

Figure 15 An Illustration Showing the Cycle of Events Regarding Flashback

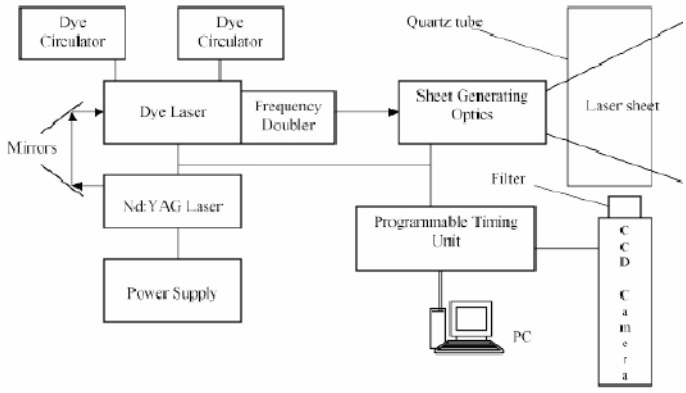

Figure 16 Schematic of the Experimental PLIF Arrangement

Image acquisition is phase locked with respect to the pressure instability cycle. Necessary phase information was determined by the upwards sloping zero crossing of the combustor pressure signal recorded by the piezoelectric transducer mounted on the combustor wall. Knowing the dominant frequency (thus the period) of oscillation a digital TTL trigger pulse was generated after the corresponding time delay for the desired phase instance. Other variables of interest (heat release, NO_x, etc.) are also simultaneously logged with the image acquisition so that their phase behavior could be investigated as well. Data logging and image triggering is orchestrated by a personal computer equipped with a data acquisition board and running LabView software, a second computer equipped with a LaVision programmable timing unit (PTU) receives the master trigger pulse generated from LabView program and triggers the Nd:Yag laser (which pumps the dye laser) and gates the ICCD camera with precise timing. Camera gating and laser light emission are synchronized with nanosecond level accuracy using dedicated timing hardware (PTU). Intensity images are recorded on this second computer. At each phase instant a total of 50 frames were recorded and averaged. For each case eight phase instances are recorded with a phase separation of 90-degrees in between. Note that zero crossings as an indicator of phase is valid if and only if the oscillatory signal is dominated by a single component [20]. In all data presented here this is the case as it can be seen from the Fourier spectra of pressure signal (see Figure 10).

Figure 17 shows phase locked OH-PLIF images of the three flow conditions investigated. Images are separated with 90 degree phase difference from each other. Intensity images are depicted with a pseudo-color scale ranging from blue to red. Red zones signify high intensity whereas blue signifies the opposite. From these OH-PLIF images the location of the flame front can be clearly identified.

Flame fronts in all of the OH-PLIF images presented exhibit a more complex topology then a simple singly connected front. This is primarily due to complex flame-vortex interactions (including the large re-circulation vortex that helps stabilize the flame) and the turbulent nature of the reacting flow under investigation. From the PLIF images it can be seen that OH signal intensity increases with increasing hydrogen content. The increased NO_x values with increasing hydrogen volume fraction (see Figure 12) can be attributed to this richer radical pool due to two specific reasons. First one is more OH signifies more heat release and thus higher temperatures which favor more rapid production of NO_x. Second one is OH radical apperars on the reactant side of some important reactions in the extended Zeldovich mechanism. This higher OH concentration in turn drives these reactions faster resulting again in a more rapid NO_x formation. Same richness in the hydroxyl radical pool can be held responsible for the extension of lean blowout limit (see Figure 4).

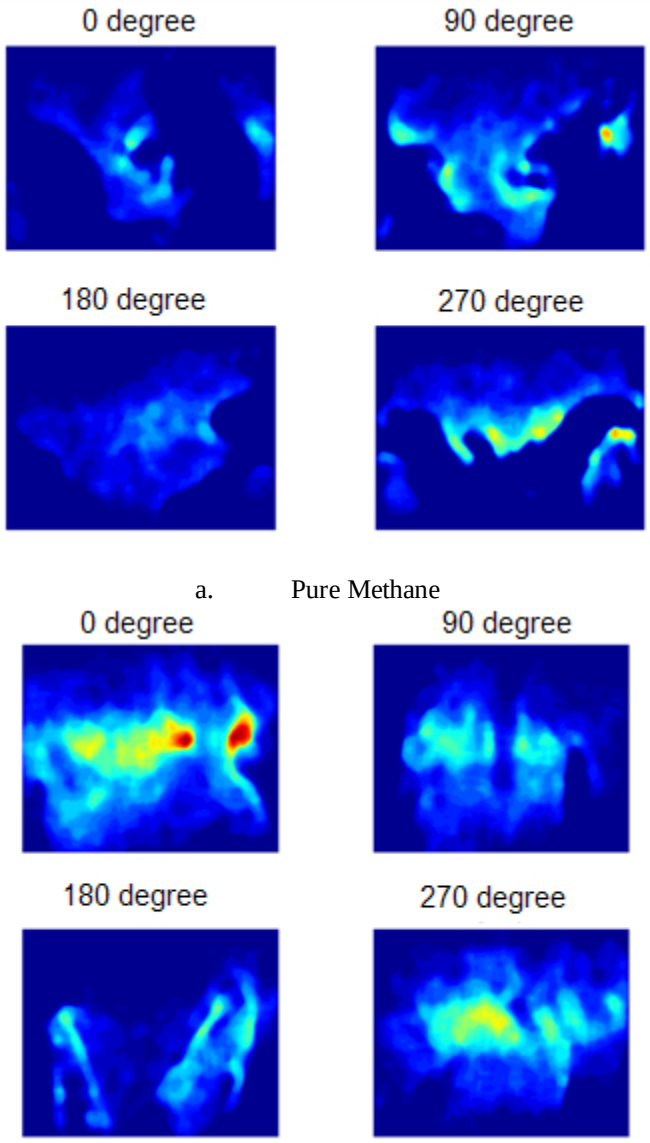

Figure 17 OH-PLIF Images

Occasionally within the OH-PLIF images presented in this section one observes regions of extinction inside the flame (i.e. Figure b 180-degrees). These local flame extinction sites are most likely caused by small scale turbulent eddies. Flame extinction can occur at these sites due to locally high strain rates causing a mismatch between the local chemical time scale and the turnover time for the local eddy.

Another set of phase locked OH-PLIF images were recorded at a higher air flow rate of Q_{air}=7.1 l/s and an equivalence ratio of ϕ=0.8 using pure methane fuel (see Figure 18). Phase locking was performed with the 100 Hz dominant instability cycle. For this particular flow condition due to higher oncoming flow velocities flame is highly strained. Since the flame is subjected to high strain rates and the flame speed is not sufficiently high a strong flame attachment cannot be observed for this flow condition. In fact, flame is only attached to the center-body (i.e. the flame holder) for less than a quarter of the whole thermo-acoustic instability cycle near the zero degree phase instant. For the rest of the instability cycle flame is de-attached from the injector and is lifted above the dump plane. Note that dump plane is located right at the bottom of these images and the center-body (which acts as a flame holder) is flush with the dump plane. Here it can be concluded that for such flow conditions front propagation is the flame stabilization mechanism. This also helps explain some of the blowout data correlations presented earlier in this paper. These result aid in the explanation of the very poor correlation between the reactor based loading parameter and blowout equivalence ratio (see Figure 6) for pure and hydrogen poor methane/hydrogen mixtures. As observed in Figure 5 fuel mixtures of such composition do correlate quite better with the flamelet based loading parameter which assumes that the flame stabilizing mechanism is through front propagation. Under this hypothesis regime blowout occurs when the local flame speed is less than the oncoming fluid velocity everywhere in the flame. Lifted flamelets can easily be identified in Figure 18.

CONCLUDING REMARKS

In this paper hydrogen-enriched confined methane combustion is studied in a laboratory scale premixed combustor. Correlating parameters for lean blowout, pressure amplitudes and emissions are examined. Two loading parameters are examined to correlate the lean blowout results: one based on a flamelet approach the other based on a well stirred reactor approach. The flamelet based loading parameter correlates better with the blowout data. Nitric oxide emissions scales with the adiabatic flame temperature. Although hydrogen enrichment increases EINO, it also enables very lean combustion. By taking advantage of the lower LBO associated with hydrogen, the combustor can be operated under very lean conditions with low flame temperature and thus favorably impact thermal nitric oxide emissions.

From the OH chemiluminescence (see Figure 11) it is seen that hydrogen enrichment shifts the flame center of mass more towards the dump plane as the burning velocity is increased with hydrogen addition. Combustion noise scales roughly with the Mach number and flame dilatation ratio.

For prospective studies PIV (particle image velocimetry) measurements are planned as an extension of this study. Results will be recorded both for mean and phase resolved velocity vectors in order to provide a better insight to the underlying flow dynamics and its interaction with chemistry.

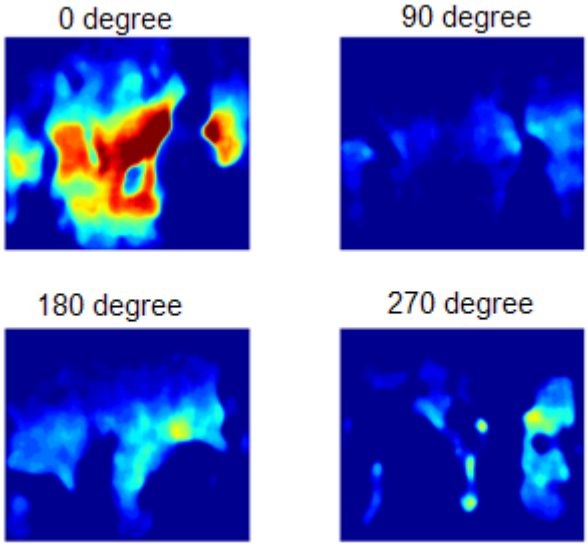

Figure 18 Phase Locked OH-PLIF Images (Q_{air}=7.1 l/s, ϕ=0.8)

NOMENCLATURE

A	Cross sectional area / Einstein coefficient for spontaneous emission
B	Einstein coefficient for stimulated absorption
C	Concentration
D	Combustor diameter
$f_{J''}$	Boltzmann fraction of the tracer species in absorbing state
g	Spectral convolution of the laser spectral distribution and the absorption transition
L	Flame height / Combustor length
M	Mach number
n_o	Number of tracer molecules
n_{tot}	Total number density
P	Pressure
Q	Rate of electronic quenching to the lower state
S	Flame speed
S_f	Fluorescence signal
T	Temperature
t	Time
U	Longitudinal velocity
V_c	Collection volume
x	Longitudinal coordinate

Greek Symbols

ϕ	Equivalence ratio / Fluorescence yield
ω	Frequency
α	Thermal diffusivity of reactants/ Hydrogen volume fraction
η	Overall efficiency of the optical setup

Subscripts

A	Air
ad	Adiabatic
f	Flame
F	Fuel
in	Inlet
L	Laminar
ref	Reference

Superscripts

$\bar{}$	Time average
$(.)'$	Fluctuating quantity

ACKNOWLEDGMENTS

This work would not be possible without the financial support obtained from Louisiana Board of Regents Clean Power and Energy Research Consortium (CPERC). Authors would like to express their gratitude for this support. The help and support received from Mr. Jeffrey Wilbanks and Mr. Jian Zhang during the experimental work is also gratefully acknowledged.

REFERENCES

1. Lawn, C. J., 1999, "Interaction of the Acoustic Properties of a Combustion Chamber with Those of Premixture Supply", Journal of Sound and Vibration, **224**, pp. 785-808
2. Zimont, V. L., 1979, "The Theory of Turbulent Combustion at High Reynolds Numbers", Combustion Explosions and Shock Waves, **15**, pp. 305-311
3. Kiesewetter, F., Hirsch, C., Fritz, M., Kroner, M., Sattelmayer, T., 2003, "Two-Dimensional Flashback Simulation in Strongly Swirling Flows", ASME Paper No: GT2003-38395
4. Dowling, A. P., 1995, "The Calculation of Thermoacoustic Oscillations", Journal of Sound and Vibration, **180**, pp. 557-581
5. Smoot, L. D., Smith, P. J., 1985, "Coal Combustion and Gasification", Plenum Press, New York
6. Tomzcak, H., Benelli, G., Carrai, L., Cecchini, D., 2002, "Investigation of a Gas turbine Combustion System Fired with Mixtures of Natural Gas and Hydrogen", IFRF Combustion Journal, Article Number: 200207
7. Cowell, L. Etheridge, C., Smith, K., 2002, "Ten Years of Industrial Gas Turbine Operating Experiences", ASME Paper No: GT-2002-30280
8. Mariotti, M., Tanzini, G., Faleni, M., Castellano, L., 2002, "Sperimentazione di Fiamme di Idrogeno a Pressione Atmosferica in un Combustore per Turbogas con Iniezione di Inerti", Technical report, Enel Produzione, Pisa, Italy, ENELP/RIC/RT/-2002/0063
9. Calvetti, S., Carrai, L., Cecchini, D., 2001, "Esecuzione di Prove di Co-Combustione di Gas Naturale e Syngas da Biomassa su un Combustore DLN per Turbina-Gas", Technical report, Enel Produzione, Pisa, Italy, ENELP/RIC/RT/-2001/258/0-IT+RT.RIC.PI
10. Calvetti, S., Carrai, L., Cecchini, D., 2001, "Progettazione di un Combustore DLN Prototipo per TG per la Co-Combustione di Gas Naturale e Syngas da Biomassa", Technical report, Enel Produzione, Pisa, Italy, ENELP/RIC/RT/-2001/146/0-IT+RT.RIC.PI
11. Tuncer, O., Acharya, S., Uhm, J. H., 2006, "Hydrogen Enriched Confined Methane Flame Behavior and Flashback Modeling", 44th AIAA Aerospace Sciences Meeting and Exhibit, Reno, Nevada, AIAA Paper No: AIAA 2006-754
12. Tuncer, O., Acharya, S., Uhm, J. H., 2006, "Effects of Hydrogen Enrichment on Confined Methane Flame Behaviour", Proceedings of ASME Power 2006, Atlanta, Georgia, ASME Paper No: PWR2006-88079
13. Beer, J. M., Chigier, N. A., 1972, "Combustion Aerodynamics", Applied Science Publishers, London, United Kingdom
14. Yu. G., Law, C. K., Wu, C. K., 1986, "Laminar Flame Speeds of Hydrocarbon Plus Air Mixtures with Hydrogen Addition", Combustion and Flame, **63**, pp. 339-347
15. Schefer, R. W., 2002, "Reduced Turbine Emissions Using Hydrogen Enriched Fuels", Proceedings of the 2002 U.S. DOE Hydrogen Program Review, NREL/CP-610-32405, pp. 1-16
16. Guo, H., Smalwood, G. J., Liu, F., Ju, Y., Gulder, O. L., 2005, "The Effect of Hydrogen Addition on Flammability Limit and NO_x Emission in Ultra-Lean Counterflow CH_4/Air Premixed Flames", Proceedings of the Combustion Institute, **30**, pp. 303-311\
17. Zhang, Q., Noble, D. R., Meyers, A., Xu, K., Lieuwen, T., 2005, "Characterization of Fuel Composition Effects in $H_2/CO/CH_4$ Mixtures Upon Lean Blowout", ASME Paper No: GT2005-68907
18. Hoffman, S., Habisreuther, P., Lenze, B., 1994, "Development and Assesment of Correlations for Predicting Stability Limits of Swirling Flames", Chemical Engineering and Processing, **33**, pp. 393-400
19. Morris, J. D., Symonds, R. A., Ballard, F. L., Banti, A., 1998, "Combustion Aspects of Application of Hydrogen and Natural Gas Fuel Mixtures to MS9001E DLN-1 Gas Turbines at Elsa Plant, Terneuzen, The Netherlands", ASME Paper No: GT98-35
20. Lieuwen, T., Zinn, B., 2000, "Investigation of Cycle to Cycle Variability in an Unstable Gas Turbine Combustor", ASME Paper No: GT2000-81
21. Morris, C. I., Kamel, M. R., Stouklov, I. G., Hanson, R. K., 1996, "PLIF Imaging of Supersonic Reacting Flows

Around Projectiles in an Expansion Tube", AIAA Paper No: AIAA-96-0855
22. Lieuwen, T., McDonell, V., Petersen, E., Santavicca, D., 2006, "Fuel Flexibility Influences on Premixed Combustor Blowout, Flashback, Autoignition and Stability", ASME Paper No: GT2006-90770
23. Tuncer, O., 2006, "Active Control of Spray Combustion", PhD Dissertation, Louisiana State University, Baton Rouge, LA